Graphene- and aptamer-based electrochemical biosensor

2014 Nanotechnology 25 205501

(http://iopscience.iop.org/0957-4484/25/20/205501)

IOP Publishing Nanotechnology
Nanotechnology 25 (2014) 205501 (8pp) doi:10.1088/0957-4484/25/20/205501

Graphene- and aptamer-based electrochemical biosensor

Ke Xu[1], Xenia Meshik[2], Barbara M Nichols[3], Eugene Zakar[3], Mitra Dutta[1] and Michael A Stroscio[1,2]

[1] Department of Electrical and Computer Engineering, University of Illinois, Chicago, IL 60607, USA
[2] Department of Bioengineering, University of Illinois, Chicago, IL 60607, USA
[3] Sensors & Electron Devices Directorate, US Army Research Laboratory, Adelphi, MD 20783, USA

E-mail: stroscio@uic.edu

Received 27 September 2013, revised 17 February 2014
Accepted for publication 19 March 2014
Published 30 April 2014

Abstract

This study investigated the effectiveness of a graphene- and aptamer-based field-effect-transistor-like (FET-like) sensor in detecting lead and potassium ions. The sensor consists of a graphene-covered Si/SiO_2 wafer with thrombin binding aptamer (TBA) attached to the graphene layer and terminated by a methylene blue (MB) molecule. K^+ and Pb^{2+} both bind to TBA and cause a conformational change, which results in MB moving closer to the graphene surface and donating an electron. Thus, the abundance of K^+ and Pb^{2+} can be determined by monitoring the current across the source and drain channel. Device transfer curves were obtained with ambipolar field effect observed. Current readings were taken for K^+ concentrations of 100 μM to 50 mM and Pb^{2+} concentrations of 10 μM to 10 mM. As expected, I_d decreased as ion concentration increased. In addition, there was a negative shift in V_{Dirac} in response to increased ion concentration.

S Online supplementary data available from stacks.iop.org/NANO/25/205501/mmedia

Keywords: DNA, field effect transistor, graphene, ion detection, thrombin binding aptamer (TBA)

(Some figures may appear in colour only in the online journal)

1. Introduction

In recent years, there has been an increasing number of studies on highly sensitive, reagentless, electrochemical biosensors based on DNA aptamers [1, 2]. While the number of aptamer-based studies is increasing, nucleic-acid-based aptamers have still been relatively insufficiently explored compared to other selectively binding molecules such as the larger amino-acid-based antibodies. In this study, a relatively small aptamer (only 15 active DNA bases)—that we have investigated in background studies addressing its basic conformational and selectivity properties [3, 4]—known as the thrombin binding aptamer (TBA), is used as the active molecular sensing element in conjunction with a graphene-based substrate. These aptamer-based electrochemical sensors potentially provide a nanoscale-sensing alternative for the detection of an extremely wide range of targets including ions, small molecules, nucleic acids, proteins, and even cells, tissues, and organisms [2]. Carbon nanotubes (CNTs), which can be visualized as crystalline carbon sheets rolled into cylindrical tubes, have attracted great attention in the development of FET-like nanosensors [5]. However, it is difficult to separate metallic CNTs from semiconducting CNTs, which is a major engineering issue in fabricating pure CNTs. In addition, due to their small interface, it is a great challenge to manipulate CNTs during device fabrication when only a few of CNTs are used. On the other hand, a flat alternative to the CNT, graphene, has large surface area and unique ambipolar characteristics which make it an effective platform for biomolecular sensing. Compared with oxide reduced graphene or exfoliated graphene, graphene films grown by chemical vapor deposition (CVD) are much better candidates for device

fabrication due to their large area, uniformity, and better reproducibility [6].

Graphene-based FETs have been demonstrated for real-time detection of various metal ions in solution. Chen *et al* [7] reported FETs using thermally reduced graphene oxide as sensing substrate to detect mercury ions. Sudibya *et al* [8]. Used micropatterned reduced graphene oxide film as sensing channel to detect different metal ions in aqueous solutions. Typically, these graphene-based FET sensors use graphene-based materials as the conducting or sensing channel, and monitor the electric signal change during the interaction between graphene and target chemicals. In this study, we demonstrated a biosensor with a graphene-based FET structure using DNA aptamers as receptors for one of the smallest possible analytes—ions. Accordingly, this study explores a prototype nanosensor for a unique array of nanosensors for small-analyte detection based on a versatile graphene platform using small molecular recognition units.

Aptamers are man-made DNA, RNA, or peptide segments which display high binding efficiency to specific targets [9]. Compared with other recognition elements such as antibodies, aptamers have a wide range of advantages such as smaller size, chemical stability, and the ability to be manufactured *in vitro* without the need for living organisms [9]. Their high binding selectivity is achieved via the systematic evolution of ligands by exponential enrichment (SELEX) method. Briefly, SELEX for DNA involves a large pool (typically 10^{13}–10^{15}) or random-sequence oligonucleotides, which are then exposed to a target molecule. The oligonucleotides that do not bind to the target are filtered out, while the rest are amplified using polymerase chain reaction. This process continues until one DNA sequence with the highest affinity for the target molecule is isolated [9]. This study used the TBA, a 15-base single-stranded DNA molecule that, in addition to the peptide thrombin, has been shown to bind to potassium and lead [3, 10]. The selectivity is due to specific cations' ability to interact with the guanines on the aptamer and stabilize the G-quadraplex structure [4]. To confirm this selective binding, TBA has been previously tested against many other metal ions, including Li^+, Na^+, Mg^{2+}, Ca^{2+}, Cu^{2+}, Ni^{2+}, Zn^{2+}, Cd^{2+}, Cr^{3+}, Al^{3+}, Hg^{2+}, Au^{3+}, and Fe^{3+} [3, 11]. These previously reported selectivity tests were taken into account in this study. Hg^{2+} has been shown to bind to symmetrical thymines on TBA, causing the aptamer to fold into a T–Hg^{2+}–T hairpin structure [11]. In this study, we focused on the detection of G-quadraplex-stabilizing ions, namely K^+ and Pb^{2+}.

The configuration of the graphene-based biomolecular sensor is schematically shown in figure 1. The aptamers are connected to the graphene surface via a linker molecule (Pyrene Cap Phosphoramidite®, Glen Research) which has a pyrene group for binding to graphene and is connected to the aptamer by phosphoramidite chemistry. Due to the overlapping of π-bonds between aromatic side chains, the pyrene group can be firmly attached to the graphene surface through π–π stacking. Methylene blue (MB) is an electron-rich electrochemical redox indicator that functions as an electron donor. Upon binding to a target molecule, the 15-base TBA, which consists of several deoxyguanosine (G) units, undergoes a conformational change and forms a G-quadraplex structure [12]. This conformational change brings the MB molecules that are attached to the other end of TBA closer to the graphene surface. When the MB molecule is in the proximity of graphene surface, it can transfer an electron to the surface and produce a readily detectable Faradaic current. This electron transfer is inhibited before the conformational change because TBA is in 'standing' position and the electron-tunneling distance is much larger. Similar aptamer-MB structure had been reported by other researchers [13–15].

This study investigated the effectiveness of the FET-like biosensor in detecting Pb^{2+} and K^+ ions. Accurate detection of these ions is important for environmental reasons and human health. Pb^{2+} is a common byproduct of industrial waste and has been known to cause significant health problems including developmental deficits in children and, in some cases, early death in adults [16]. K^+ is an essential ion that regulates cell signaling in living organisms, and human blood serum K^+ levels above or below the 3.5–5 mM range are cause for concern [17]. Thus, an effective sensor for Pb^{2+} and K^+ would be greatly beneficial.

2. Experiment

2.1. Fabrication of graphene-based biosensor

Graphene samples were originally grown on copper foil using low pressure chemical vapor deposition. Growths were performed at 1025°C for 30 min at 0.5–0.6 Torr pressure using hydrogen and methane as the carrier and carbon feedstock gases. The hydrogen/methane gas flow ratio for the growths ranged from 2.5 to 1.5. In order to transfer the graphene sheet to a Si/SiO_2 substrate, the copper foil was coated with poly(methylmethacrylate) (PMMA) and went through an O_2 plasma ashing process to remove backside graphene. After wet etching of the copper foil, the PMMA/graphene sheet was transferred onto an n^{++} Si substrate coated with 296 nm of SiO_2. The thickness of the Si wafer is 525 μm. Finally, PMMA was removed by soaking in chloroform. Raman characterization of the graphene after transfer was performed using a Renishaw inVia Raman microscope with an excitation laser wavelength of 514 nm. In lieu of precise mapping, Raman spectra were taken at multiple points over a 60×40 μm area and the characteristic graphene peaks were fitted using the Lorentz peak approximation. The graphene films consisted mostly of single layer graphene with small amounts of bilayer graphene present (9–11%).

The FET-like structure was fabricated on thegraphene surface using optical lithography. 45 nm thick gold and 5 nm thick chromium were deposited on the graphene sheet as source and drain electrodes using electron beam evaporation. Source and drain were patterned by photoresist mask and chemical etching technique. Owing to the large size and good uniformity of the CVD grown graphene film, we were able to fabricate nine identical electrodes on the same substrate available for multi-channel detection. This also enabled us to

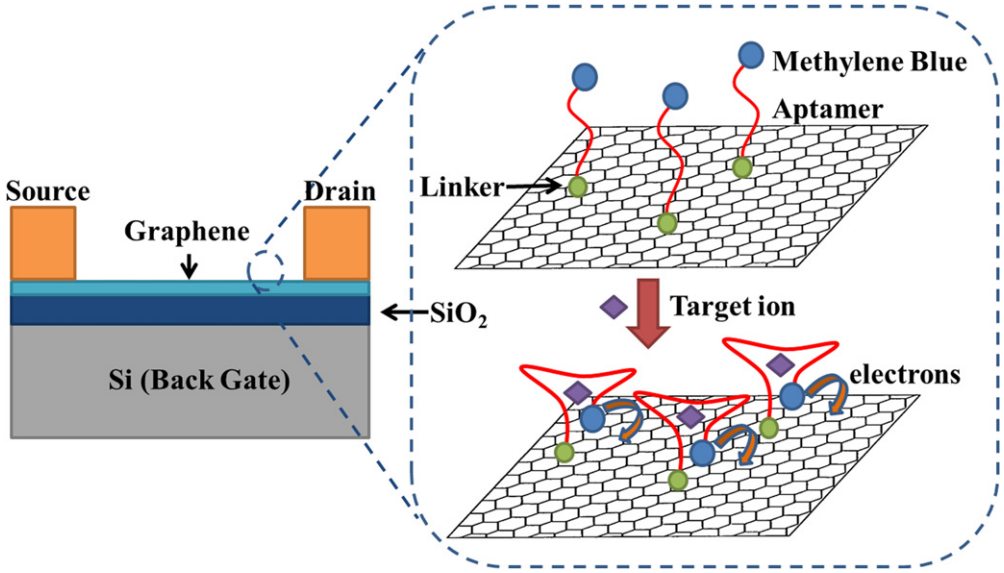

Figure 1. Schematic illustration of graphene-based biosensor.

perform device characteristic measurements and device performance comparisons without being affected by artifacts from discrete flakes. The length and width of the channel were both set to 2 mm for ease-of-use as a biomolecule sensor in the future. The Si wafer was degenerately doped with a conductivity of 0.005 Ω cm and used as the global backgate.

2.2. Synthesis of control structures for optical experiments

The ability of DNA to bind to graphene via a pyrene group was tested by first synthesizing a control structure, where MB was replaced with a fluorescent quantum dot (QD). Since QDs are fluorescent, the binding of TBA-QD to graphene can be confirmed via optical microscopy. Thus, the control structures were used in the preliminary step of the experiment to confirm the aptamer's ability to bind to graphene via the pyrene group. TBA with 5′ pyrene and 3′ amine modifications (5′-/Pyrene /GGTTGGTGTGGTTGG/AminoC12/-3′) was purchased from Biosearch Technologies, Inc. (Novato, CA). Carboxyl-functionalized eFluor 700NC InGaP QDs were purchased from eBioscience, Inc. (San Diego, CA) and conjugated to TBA. To achieve the conjugation, the QDs were first exchanged into 0.1 M 2-(N-morpholino) ethanesulfonic acid buffer via a 100 K Nanosep® molecular weight cutoff (MWCO) device (Life Sciences, Ann Arbor, MI). Carboxyl groups on the QDs were activated with 1-Ethyl-3-(3-dimethylamino propyl) carbodiimide hydrochloride (EDC) (Pierce Biotechnology, Rockford, IL) and N-hydroxysulfosuccinimide (Sulfo-NHS) (Pierce Biotechnology, Rockford, IL). A 100 K MWCO device was then used to filter out EDC and Sulfo-NHS and buffer exchange the solution into low-sodium phosphate-buffered saline (PBS). TBA was added to the activated QDs at a 1:10 QD:TBA ratio, and the mixture was spun gently at room temperature for 2 h. Finally, the conjugate was filtered using a 100 K MWCO device to remove unbound TBA.

Before attaching the TBA-QD conjugate to graphene, the wafer was washed in acetone and deionized H_2O. TBA-QD was buffer exchanged into anhydrous dimethylformamide (DMF) (Sigma-Aldrich, St. Louis, MO). A 15 μM drop of TBA-QD was placed on the graphene and incubated for 2 h. The wafer was then rinsed thoroughly with diH_2O to remove unbound conjugates. Plain QDs were also incubated on the graphene using the concentration and procedure described above. The samples were viewed using Nikon Eclipse E600 microscope. Raman spectroscopy was also performed on the samples to verify the presence of DNA on the graphene.

2.3. Synthesis of FET-like sensor with DNA and MB

TBA with 5′ pyrene and 3′ methylene blue modifications (5′-/Pyrene /GGTTGGTGTGGTTGG/Methylene Blue/-3′) was purchased from Biosearch Technologies, Inc. (Novato, CA). A 15 μM drop of TBA in anhydrous DMF was placed on the wafer between two contacts and left to incubate for 2 h. The wafer was then washed twice with diH_2O, to remove unbound TBA and leave only the TBA that is attached to graphene via pyrene linker. Pb(II)Cl_2, KCl, and NaCl were dissolved in diH_2O to obtain solutions of various ion concentrations. 5 μL drops of ion solution were placed on the wafer on the spot occupied by TBA, and probes were placed on the adjacent contacts.

All electrical measurements were conducted at room temperature using a precision semiconductor parameter analyzer (Agilent, 4156B). In order to have better contact on the interface, a 8060 MicroManipulator Probing System was used to connect the semiconductor parameter analyzer with the sample surface. The electrodes remain dry during all electrical measurements.

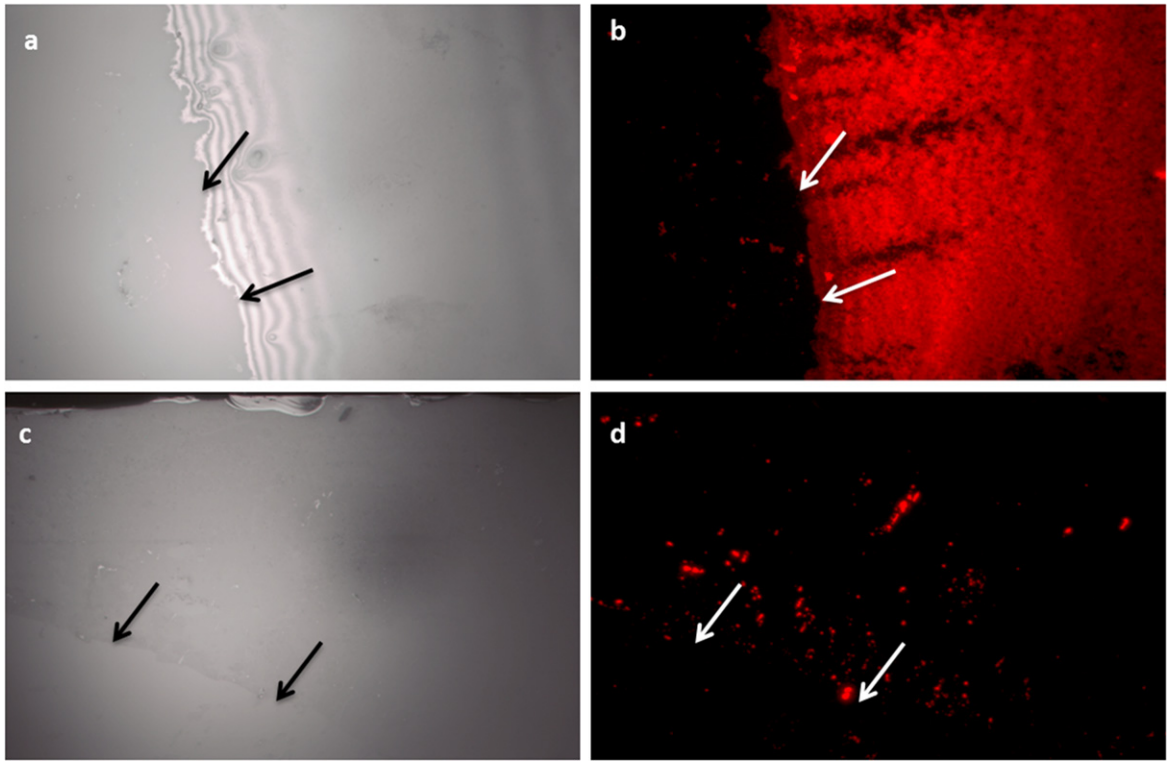

Figure 2. Microscope images of graphene wafers after 2 h incubation with TBA-QD or plain QD after a thorough rinse with diH_2O. Arrows indicate the edge of the graphene flake. (a) Bright field image of graphene with TBA-QD. (b) Fluorescent image of graphene with TBA-QD. (c) Bright field image of graphene with plain QDs. (d) Fluorescent image of graphene with plain QDs.

3. Results and discussion

3.1. Optical verification of DNA-graphene bonding

Figure 2 shows the attachment of TBA-QD to graphene compared to plain QDs. Red fluorescence indicates the presence of QDs. The fluorescence intensity in figure 2(b) is clearly higher than in figure 2(d), demonstrating that a significant number of QD-TBA molecules remained on the graphene even after the wafer was rinsed with diH_2O. Plain QDs, in contrast, were largely removed by the rinsing process consisting of two rinse cycles. In addition, the edge of the graphene flake is visible in figure 1, and TBA-QD clearly binds to graphene only. These results demonstrate that pyrene successfully binds to graphene and can be used as an effective linker for the FET-like sensor. Raman results (not shown) also confirm binding of TBA to graphene with the presence of several peaks in the 900–1600 cm^{-1} range, which is consistent with typical wavenumbers for DNA peaks [18]. This proof of binding, obtained through the use of TBA-QD control structures, allowed us to proceed to the main part of the experiment—the FET-like sensor with TBA aptamer and MB.

3.2. Device characteristic

As shown in figure 3, the conductance of dry, unfunctionalized graphene-based FET-like devices resembles the ambipolar field effect in semiconductors. The source-drain voltage is set constant at 10 mV and 25 mV, respectively. Mathematical curve-fitting was used to remove noise. Conductivity

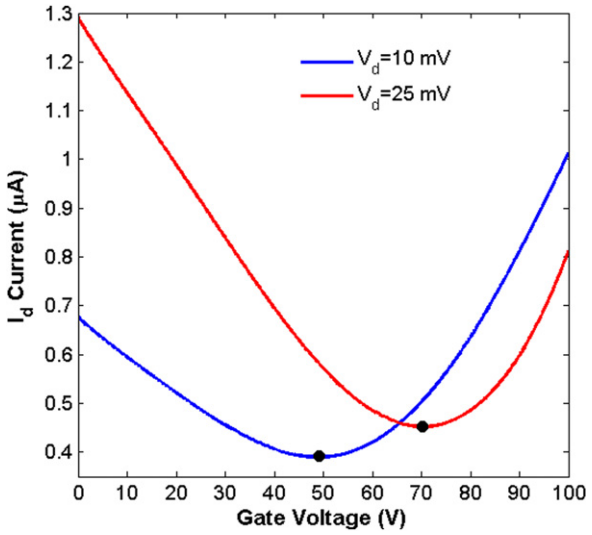

Figure 3. Device transfer curves of two graphene-based FET-like structures.

increases with V_g on both sides of the minimum conductance point. The device transfer curves (drain current I_d versus gate voltage V_g) of the multiple graphene-based structures were found to be quite reproducible. The minimum conductance points were always in the positive backgate voltages, between 50 V to 70 V. The standard deviation of the gate voltage for minimal conductance point under the drain voltage of 10 mV and 25 mV are 0.72 V and 0.60 V, respectively. The location of minimum conductance point or Dirac point can be used to

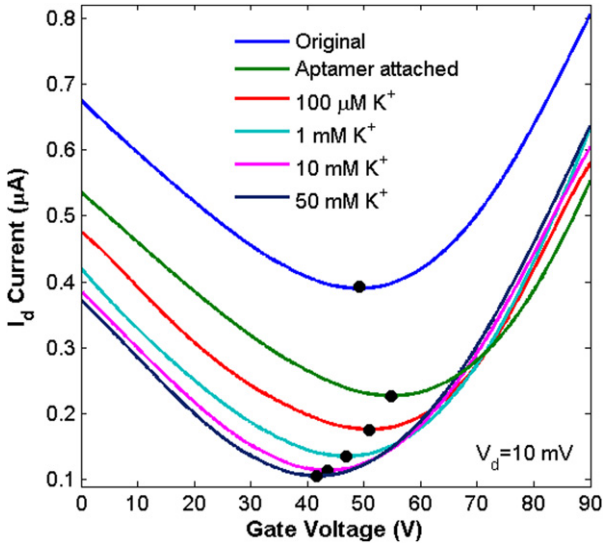

Figure 4. Device transfer curves of the original FET-like structure, the structure after aptamer attachment, and after adding different concentrations of K^+ ions.

monitor the doping state of thegraphene film. The shift of Dirac point voltage (V_{Dirac}) from zero to large positive V_g indicates that the graphene behaves like a degenerately doped p-type semiconductor without electric field doping (at zero V_g). This shift is also found by other research groups and can be attributed to unintentional doping by absorbed water in ambient conditions [19] as well as impurities adsorbed to the graphene during the fabrication process [20]. It is possible that the negatively-charged impurities originated from the transfer process on the SiO_2 substrates are trapped underneath graphene layer and lead to intrinsic p-doping effect in the graphene [21]. The drain source currents (I_d) are in the range of 0.39–0.80 μA and 0.45–1.29 μA, respectively, and the current on–off ratio is about 2. In this paper we used the current change after introduction of ions as an indication of detecting target ions. Single layer graphene has the unique electronic ability to be able to operate in both p-type and n-type conduction region (detailed discussion in section 3.3). The FET performance as shown in the device transfer curves allowed us to monitor the current changes in both conduction regions.

3.3. Graphene-based biomolecular sensor

The location of V_{Dirac} is sensitive to the immobilization of DNA aptamer structures. The green curve in figure 4 shows the device transfer curve after the aptamer structure was attached on the graphene surface. As compared to the blue curve from original device, the I_d current decreased and V_{Dirac} right-shifted after the aptamer structures were introduced to the device. This is possibly due to the non-covalent functionalization process of the DNA aptamer. Although the relatively weak π–π stacking or van der Waals interaction can preserve the superb physical properties of graphene, it has been demonstrated that functionalization with pyrene groups can cause V_{Dirac} to shift significantly towards the right, indicating a typical p-type doping behavior [22]. Huang *et al* also discovered a current decrease and right-shift after functionalizing graphene surface with linker molecules consisting pyrene groups [23].

In order to understand the use of this device as a biomolecular sensor, it is necessary to consider the underlying principles by which the graphene-based biosensor functions. Large-area-graphene transistors are known to have unique current–voltage transfer characteristics as shown in figure 3. The transfer curve can be divided into two branches separated by the Dirac point which is the minimum conductance point. The type of carrier and carrier density in the channel are modulated by the potential difference between the gate and the channel. On the right side of the Dirac point where large positive gate voltages are applied, electrons accumulate and form an n-type conduction channel. On the left side of the Dirac point, negative gate voltage (compared to V_{Dirac}) lead to a p-type conduction channel where holes are the majority carrier.

As shown in figure 4, the device transfer curve changed after different concentrations of K^+ were added into the sensor. To be specific, after adding 100 μM concentration of K^+ (red curve), the current in the channel decreased in the range of 0–51.1 V gate voltage. This is because the device is working in the p-type conduction region with holes as the majority carriers. When K^+ is introduced into the structure, aptamers undergo conformational change and bring MB close to the surface. The excess electrons transferred from MB will decrease the carrier concentration in the channel and cause a current decrease. On the other hand, when gate voltage is greater than V_{Dirac}, the device works in the n-type conduction region and the external electron charges will lead to an increase in carrier concentration as well as an increase in the current. This explains the rise of current after 51.1 V gate voltage. The current decrease in the p-type conduction region and current increase in the n-type conduction region proves that we have successfully detected K^+ ions.

It is worth noting that aside from current change V_{Dirac} also shifted from 54.9 V (green curve) to 51.1 V (red curve). As discussed previously the left-shift of V_{Dirac} can be the result of the n-doping effect. Electrical contacts to a graphene surface have been found to exhibit high resistance [24]. Weak electron conduction at the contact-graphene interface can cause the external electrons provided by MB to be trapped on the graphene surface [25]. It's likely that the electron transfer and electron accumulation induced an n-doping effect inside graphene. Similar negative shift of V_{Dirac} had been reported by Chen *et al* after functionalizing graphene with short DNA strands [4]. They attributed the n-doping effect to the interaction between graphene and electron-rich nucleobases in DNA molecules.

The transfer curve continues to shift with the increasing concentration of K^+. The initial current I_0 (when no gate voltage is applied), minimum conduction current and V_{Dirac} position at different K^+ concentrations are shown in table 1. After adding 50 mM of K^+, the minimum conduction current dropped by about 51.2%.

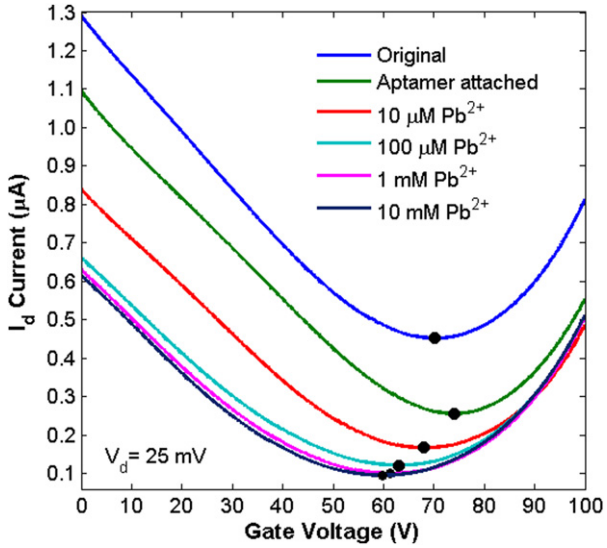

Figure 5. Device transfer curve of the original FET-like structure, the structure after aptamer attachment, and after adding different concentrations of Pb^{2+} ions.

Table 1. I_0, V_{Dirac} and minimum conduction current at different K^+ concentrations.

I_d at different conditions	I_0 (μA)	V_{Dirac} (V)	Minimum conduction current (μA)
Original device	0.6749	49.2	0.3921
Aptamer structure attached	0.5355	54.9	0.2272
100 μM K^+ added	0.4757	51.1	0.1758
1 mM K^+ added	0.4202	46.9	0.1370
10 mM K^+ added	0.386	43.6	0.1185
50 mM K^+ added	0.3718	41.8	0.1109

In order to investigate the effectiveness of the device in detecting Pb^{2+}, another graphene-based biosensor was fabricated with identical structure. Figure 5 shows the transfer curve changes with the increases in Pb^{2+} concentration. Similar changes have been observed as in the K^+ detection measurement, indicating consistent performance of the device.

Data for the initial current I_0, minimum conduction current and V_{Dirac} position at different Pb^{2+} concentrations are shown in table 2. The minimum conduction current dropped about 62.7% after adding 10 mM of Pb^{2+}.

The sensor appears to be more sensitive to Pb^{2+}, showing a 62.7% signal decrease for 10 mM Pb^{2+}, versus 47.8% for the same concentration of K^+. In addition, adding as little as 10 μM of Pb^{2+}causes the signal to decrease about 35%, while it takes nearly 1 mM of K^+ to reach the same signal decrease. Based on the calibration curves depicting the relationship between minimum conduction current and target ion concentration (see supporting information, figure S1), the sensor appears to be more sensitive to K^+ concentrations below 10 mM and Pb^{2+} concentrations below 2 mM. For concentrations above these values, the signal saturates between

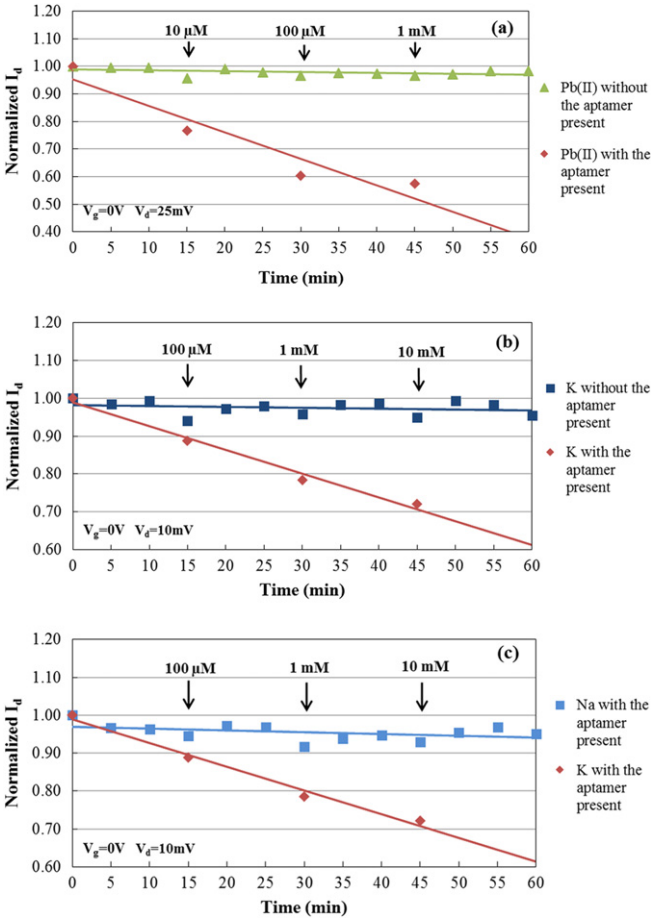

Figure 6. Normalized drain current (I_d) after the introduction of (a) Pb^{2+} ions without the aptamer present, (b) K^+ ions with the aptamer present and (c) Na^+ ions with the aptamer present. Data from previous sensor experiments were plotted alongside for comparison.

Table 2. I_0, V_{Dirac} and minimum conduction current at different Pb^{2+} concentrations.

I_d at different conditions	I_0 (μA)	V_{Dirac} (V)	Minimum conduction current (μA)
Original device	1.29	70.3	0.4522
Aptamer structure attached	1.095	74.1	0.2562
10 μM Pb^{2+}added	0.8391	68.2	0.1673
100 μM Pb^{2+} added	0.661	63.1	0.1219
1 mM Pb^{2+} added	0.6291	61.5	0.1003
10 mM Pb^{2+} added	0.6147	59.9	0.0956

0.1 and 0.15 μA. Therefore, a linear trendline was fitted to the first three data points to estimate the sensor's sensitivity in its most sensitive region. According to the trendline equations, the sensitivity in this region is around 0.09 μA mM^{-1} for K^+ and 1.4 μA mM^{-1} for Pb^{2+}. The same calibration curves were used to estimate the detection limit. Based on the limitations of the semiconductor parameter analyzer used in the *I–V* measurements, the minimum detectable current change was

Table 3. Comparison with commercially available sensors.

Sensor	Target ion	Detection range	Sensitivity/resolution
FET-like aptamer-based sensor (described in this work)	K^+	27 μM–10 mM	0.09 μA mM^{-1}
	Pb^{2+}	2 μM–2 mM	1.4 μA mM^{-1}
B-731 LAQUAtwin compact potassium ion meter, HORIBA (B-731)	K^+	1–100 mM	Resolution: 26 μM (for 1–2.5 mM range) 256 μM (for 2.5–25 mM range) 2.56 mM (for 25–100 mM range) [26]
Lead ion electrode, Horiba (8008-10C)	Pb^{2+}	10 μM–100 mM	N/A [27]
Orion lead electrode, Thermo Scientific (9482BN)	Pb^{2+}	>1 μM	25–30 mV for every decade change concentration [28]

determined, and the linear trendline equations were used to extrapolate the ion concentrations that would yield this current. The detection limit was thus calculated to be 27 μM for K^+ and 2 μM for Pb^{2+}.

The sensor's sensitivity is comparable to several commercially available sensors (table 3). While our sensor cannot accurately detect high concentrations on the mM scale, its lower detection limit is comparable with and, in some cases, lower than other commercially available sensors, and the sensitivity is quite high at low ion concentrations. Like other sensors, it functions best at neutral pH. Although one drawback is irretrievability of the sample, an advantage is the extremely small required sample volume (~1 μL or less).

Buffer characteristics can affect the sensor's sensitivity. Hianik *et al* reported on the effect of buffer pH and ionic strength on the binding efficiency of TBA to its target peptide, thrombin. A pH of 7.5 was determined to be optimal for binding, with the sensitivity decreasing significantly for higher and lower pH values. This is likely because the pH influences the structure of TBA's binding site, altering its binding ability. A pH of 7.5 is a convenient value for optimal sensor function, as it is close to physiological pH and the pH of water.Similarly, the sensitivity decreases with increasing NaCl concentrations, indicating that TBA functions optimally in buffers with low ionic strength. A likely explanation for this is that in high ionic strength buffers, the ions shield the negative charges on the DNA, making it harder for the aptamer to bind to its positively charged targets [29]. It is therefore best to use the sensor for samples with minimal amounts of non-target ions. Nevertheless, previous work by our group has shown that TBA-based sensors undergo the binding-induced conformational change in a variety of buffers, including PBS buffer [3], TE (10 mM Tris, 1 mM EDTA, pH 8.0) buffer [10, 30], and physiological fluids such as urine [4].

The stability and selectivity of the biosensor was investigated by control experiments. Since the sensors are irreversible, it is not possible to conduct control experiments on the same functionalized sensors. Instead we designed three separate control experiments. In the first two experiments, K^+ and Pb^{2+} ions were introduced to the pure graphene-based FET-like structure without aptamers, respectively. In the third experiment, sodium ions were introduced to the aptamer-MB functionalized biosensor. Drain voltages in the control experiments were set at the same values as previous sensor experiments. To have a better look of the current change on control structures, we conducted control experiments with no gate voltage applied and monitored the time dependent response of drain current after the introductions of target ions. Figure 6 shows the normalized drain current as a function of time after the introduction of target ions with various concentrations. In order to have a good comparison, data from previous sensor experiments (I_0) were plotted alongside with data from control experiments. Since the control experiments were conducted in separate control structures, the initial current values (before ion addition) were different in each experiment. Thus we normalized the currents with respect to their initial values so that after normalization all the currents start at 1. This normalization ensures that all three control experiment results are consistent and comparable. Without the TBA-MB structure, K^+ and Pb^{2+} ions were not able to cause sharp current decreases as they did in TBA-MB functionalized biosensors. Similarly, after adding sodium ions to the aptamer-MB functionalized biosensor, the drain current only exhibits a slight change, indicating a weak dependence of channel conductance with sodium concentrations. Comparing the lack of responses from control experiments and sharp current decrease from functionalized sensor measurements, we determined that the graphene-based biosensor is a good tool for the detection of both K^+ and Pb^{2+} ions.

4. Conclusion

This study introduced a novel FET-like biosensor and proved its effectiveness in detecting K^+ and Pb^{2+} ions. It can potentially detect K^+ concentrations as low as 27 μM and 2 μM concentrations of Pb^{2+}. The information in our paper is potentially useful for a whole class of nanosensors for detecting small analytes (much smaller than feasible with antibodies) based on a nanoscale graphene platform. Since detection of K^+ and Pb^{2+} at these concentrations is of the utmost importance for environmental and health reasons, the sensor can potentially be used in medical or industrial settings.

Acknowledgements

This work was supported by Army Research Office (ARO) through MURI grant W911NF-11-1-0024.

References

[1] White R, Rowe A and Plaxco K 2010 Re-engineering aptamers to support reagentless, self-reporting electrochemical sensors *Analyst* **135** 589–94
[2] Lee J, So H, Jeon E, Chang H, Won K and Kim Y 2008 Aptamers as molecular recognition elements for electrical nanobiosensors *Anal. Bioanal. Chem.* **390** 1023–32
[3] Wu T, Biswas S, Dutta M and Stroscio M 2011 Quantum-dot-based aptamer beacon for the detection of potassium ions *IEEE Trans. Nanotechnol.* **10** 991–5
[4] Wu T C, Zhao G J, Lu H, Dutta M and Stroscio M A 2013 Quantum-dot-based aptamer beacons for k+ detection *IEEE Sensors J.* **13** 1549–53
[5] Maehashi K and Matsumoto K 2009 Label-free electrical detection using carbon nanotube-based biosensors *Sensors* **9** 5368–78
[6] Chen T, Phan T, Hsu C, Lee Y, Wang J, Wei K, Lin C and Li L 2013 Label-free detection of DNA hybridization using transistors based on CVD grown graphene *Biosens. Bioelectron.* **41** 103–9
[7] Chen K, Lu G, Chang J, Mao S, Yu K, Cui S and Chen J 2012 Hg(II) ion detection using thermally reduced graphene oxide decorated with functionalized gold nanoparticles *Anal. Chem.* **84** 4057–4062
[8] Sudibya H G, He Q, Zhang H and Chen P 2011 Electrical detection of metal ions using field-effect transistors based on micropatterned reduced graphene oxide films *ACS Nano* **5** 1990–4
[9] Keefe A, Pai S and Ellington A 2010 Aptamers as therapeutics *Nat. Rev. Drug Discovery* **9** 537
[10] Brenneman K, Poduri S, Stroscio M and Dutta M 2013 Optical detection of lead(II) ions using DNA-based nanosensor *IEEE Sensors J.* **13** 1783–6
[11] Liu C, Huang C and Chang H 2009 Highly selective DNA-based sensor for lead(II) and mercury(II) ions *Anal. Chem.* **81** 2383–7
[12] Liu W, Fu Y, Zheng B, Cheng S, Li W, Lau T and Liang H 2011 Kinetics and mechanism of conformational changes in a G-Quadruplex of thrombin-binding aptamer induced by Pb2+ *J. Phys. Chem.* B **115** 13051–6
[13] Xiao Y, Piorek B D, Plaxco K W and Heeger A J 2005 A reagentless signal-on architecture for electronic, aptamer-based sensors via target-induced strand displacement *J. Am. Chem. Soc.* **127** 17990–1
[14] Baker B R, Lai R Y, Wood M S, Doctor E H, Heeger A J and Plaxco K W 2006 An electronic, aptamer-based small-molecule sensor for the rapid, label-free detection of cocaine in adulterated samples and biological fluids *J. Am. Chem. Soc.* **128** 3138–9
[15] Radi A, Sánchez J L A, Baldrich E and O'Sullivan C K 2006 Reagentless, reusable, ultrasensitive electrochemical molecular beacon aptasensor *J. Am. Chem. Soc.* **128** 117–24
[16] Rossi E 2008 Low level environmental lead exposure–a continuing challenge *Clin. Biochem. Rev.* **29** 63–70
[17] Kratz A, Ferraro M, Sluss P M and Lewandrowski K B 2004 Case records of the massachusetts general hospital.weekly clinicopathological exercises. laboratory reference values *N Engl. J. Med.* **351** 1548–63
[18] Otto C, Vandentwell T, Demul F and Greve J 1986 Surface-ehanced Raman-spectroscopy of DNA bases *J. Raman Spectrosc.* **17** 289–98
[19] Novoselov K, Geim A, Morozov S, Jiang D, Zhang Y, Dubonos S, Grigorieva I and Firsov A 2004 Electric field effect in atomically thin carbon films *Science* **306** 666–9
[20] Meric I, Han M, Young A, Ozyilmaz B, Kim P and Shepard K 2008 Current saturation in zero-bandgap, topgated graphene field-effect transistors *Nat. Nanotechnology* **3** 654–9
[21] Shi Y, Dong X, Chen P, Wang J and Li L 2009 Effective doping of single-layer graphene from underlying SiO_2 substrates *Phys. Rev.* B **79** 115402
[22] Mao H, Lu Y, Lin J, Zhong S, Wee A and Chen W 2013 Manipulating the electronic and chemical properties of graphene via molecular functionalization *Prog. Surf. Sci.* **88** 132–59
[23] Huang Y, Dong X, Shi Y, Li C, Li L and Chen P 2010 Nanoelectronic biosensors based on CVD grown graphene *Nanoscale* **2** 1485–8
[24] Robinson J, LaBella M, Zhu M, Hollander M, Kasarda R, Hughes Z, Trumbull K, Cavalero R and Snyder D 2011 Contacting graphene *Appl. Phys. Lett.* **98** 053103
[25] Xu K, Qian J, Shukla P, Dutta M and Stroscio M 2012 Graphene-based FET structure: modeling FET characteristics for an aptamer-based analyte Sensor *IEEE Conf. Proc. of 15th Int. Workshop on Computational Electronics* doi:10.1109/IWCE.2012.6242868
[26] http://www.horiba.com/us/en/application/material-property-characterization/water-analysis/water-quality-electrochemistry-instrumentation/compact/details/b-731-laquatwin-compact-potassium-ion-meter-17163/
[27] http://www.horiba.com/application/material-property-characterization/water-analysis/water-quality-electrochemistry-instrumentation/electrodes-accessories/ion-electrodes/details/lead-ion-electrode-8008-10c-9519/
[28] http://www.thermoscientific.com/content/dam/tfs/ATG/EPD/EPD%20Documents/ Product%20Manuals%20&%20Specifications/Water%20Analysis%20Instruments%20and%20Supplies/Lab%20Electrodes%20and%20Sensors/Ion%20Selective%20Electrodes/D17172~.pdf
[29] Hianik T, Ostatna V, Sonlajtnerova M and Grman I 2007 Influence of ionic strength, pH and aptamer configuration for binding affinity to thrombin *Bioelectrochemistry* **70** 127–33
[30] Brenneman K L, Sen B, Stroscio M A and Dutta M 2010 Aptamer-based optical bionanosensor formercury (II) ions *IEEE Nanotechnology Materials and Devices Conf.* pp 221–4